Semantic UE Localization for OFDM Transceiver Systems

Hyunwoo Park*, Adam Dubs*, Andrea Conti†, Sunwoo Kim*, and Moe Z. Win‡
*Department of Electronic Engineering, Hanyang University, South Korea
†Department of Engineering and CNIT, University of Ferrara, Italy
‡Laboratory for Information and Decision Systems, Massachusetts Institute of Technology, USA

***Abstract*—This paper proposes a semantic localization method for orthogonal frequency division multiplexing (OFDM) transceiver systems with analog beamforming that simultaneously estimates user equipment (UE) position and classifies UE type. The proposed approach employs beam sweeping at both transmitter and receiver to extract angle and range information from reflected signal paths. The received signals undergo appropriate preprocessing before being fed into a classification network to distinguish between human and robotic UE. The classification capability stems from aperture-dependent scattering characteristics inherent to different UE types, which manifest as distinguishable features in the received signal domain. Simulation results demonstrate successful localization and type classification, enabling radio-based environmental awareness for location-based services and digital twin applications.**

***Index Terms*—Semantic sensing, localization, OFDM, UE classification, beamforming.**

I. Introduction

Semantic information, encompassing both positional data and object type attributes, is becoming critical for beyond-5G and 6G wireless networks [1]. While conventional localization focuses solely on position estimation, integrating semantic awareness unlocks new possibilities for location-based services and digital twin construction [2]. Radio-based semantic localization, which simultaneously determines user equipment (UE) position and classifies UE type through wireless signals, presents a transformative opportunity for comprehensive environmental awareness in next-generation networks [3].

Existing localization methods for orthogonal frequency division multiplexing (OFDM) systems primarily extract angle-of-arrival (AOA) and time-of-arrival (TOA) information through channel estimation [4] or beam-based approaches [5]–[7]. However, these methods address only position estimation without distinguishing UE types. Recent advances demonstrate that different object types exhibit distinct electromagnetic scattering characteristics [8], yet their integration semantics remain unexplored. Additionally, radar-based object tracking and classification research exists [9], but it uses dedicated radar signals rather than communication waveforms, precluding simultaneous data transmission.

The fundamental research described in this paper was supported, in part, by the Institute of Information & Communications Technology Planning & Evaluation of Korea under Grant RS-2024-00428780, and by the Robert R. Taylor Professorship. *(Corresponding authors: Sunwoo Kim and Moe Z. Win)*

This paper proposes a semantic localization method that simultaneously estimates UE position and classifies UE type by exploiting aperture-dependent scattering characteristics. The proposed method employs beam sweeping at transmitter and receiver to obtain angle and range information from reflected paths. Received signals are preprocessed and fed into a classification network to distinguish human and robotic UE based on their distinguishable scattering patterns. Simulation parameters are configured to match practical mmWave transceiver system specifications, ensuring direct testbed applicability. Performance evaluation encompasses both position-related parameter estimation accuracy across different UE types and classification accuracy under various conditions. The main contributions are:

- the semantic localization method for analog beamforming OFDM transceiver testbeds, enabling joint position estimation and UE type classification.
- the classification framework exploiting aperture-dependent scattering characteristics to distinguish UE types from received signal features.
- validation demonstrating localization accuracy and classification performance for radio-based environmental awareness.

Notations: For a matrix $\mathbf{A}$, its Hermitian transpose and transpose are respectively denoted as $\mathbf{A}^{\mathsf{H}}$ and $\mathbf{A}^{\top}$. The notation $\mathcal{CN}(\boldsymbol{\mu}, \boldsymbol{\Sigma})$ denotes the circularly symmetric complex Gaussian distribution of a random vector with mean vector $\boldsymbol{\mu}$ and covariance matrix $\boldsymbol{\Sigma}$. $\mathbf{I}$ denotes the identity matrix. The symbol $\imath$ represents the imaginary unit of complex numbers, ($\imath = \sqrt{-1}$). $\|\cdot\|$ returns Euclidean norm.

II. System Model

Consider an OFDM transceiver system, where transmitter (Tx) and receiver (Rx) are communicating each with N antennas. Each user is equipped with a single antenna and located in a 2-dimensional (2D) space with origin given by the base station (BS) extremely large aperture array (ELAA) and exhibits distinct reflection characteristics depending on their unknown user type. Let $\mathbf{p}_l \in \mathbb{R}^{2\times 1}$ denotes the position of the l-th UE, and $\dot{\mathbf{p}}_{i,l} \in \mathbb{R}^{2\times 1}$ denotes the position of the i-th scattering point associated with the l-th UE. For semantic UE localization, the Tx and Rx perform beam sweeping and the Rx receives the beam sweeping results as in Fig. 1.

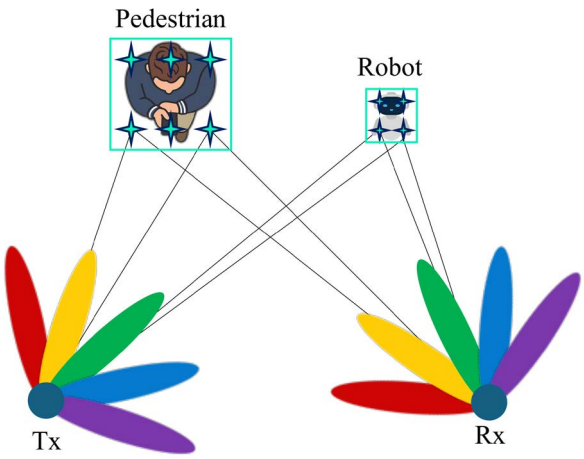

Fig. 1. Considered semantic UE localization scenario.

The beam sweeping result for the m-th subcarrier $\mathbf{Z}_m \in \mathbb{C}^{N\times N}$ is expressed as

$$\mathbf{Z}_m = \mathbf{W}^\top \mathbf{H}_m \mathbf{F} s_m + \boldsymbol{\eta}_m \tag{1}$$

where $\mathbf{W} \in \mathbb{C}^{N\times N_\mathrm{B}}$ is the combining matrix with N_B representing the number of beams, $\mathbf{H}_m \in \mathbb{C}^{N\times N}$ is the channel between Tx and Rx, $\mathbf{F} \in \mathbb{C}^{N\times N_\mathrm{B}}$ is the precoding matrix, s_m is the tranmited signal for sensing satisfying $\mathbb{E}(|s_M^2|) = 1/M$, and $\boldsymbol{\eta}_m$ is the additive white Gaussian noise. The combining matrix $\mathbf{W}$ and precoding matrix $\mathbf{F}$ are constructed from uniform linear array (ULA) steering vectors, expressed as

$$\mathbf{W} = \mathbf{F} = [\, \mathbf{a}(\phi_1)\ \mathbf{a}(\phi_2)\ \ldots\ \mathbf{a}(\phi_{N_\mathrm{B}})\,] \tag{2}$$

where $\mathbf{a}(\phi) = [1, e^{j\pi\cos(\phi)}, \ldots, e^{j\pi(N-1)\cos(\phi)}]^\top \in \mathbb{C}^{N\times 1}$ denotes the steering vector for angle ϕ. The angles $\{\phi_i\}_{i=1}^{N_\mathrm{B}}$ are uniformly distributed over $[30°, 150°]$.

The channel matrix $\mathbf{H}_m$ models the multi-path propagation from UE reflections under line-of-sight (LOS) blockage conditions, given by

$$\mathbf{H}_m = \sum_{l=1}^{L}\sum_{i=1}^{I_l} \sqrt{\dot{\beta}_{i,l,m}}\, \mathbf{h}_{i,l,m,\mathrm{Rx}} \mathbf{h}_{i,l,m,\mathrm{Tx}}^\top \tag{3}$$

where I_l is the number of scattering points of the UE l, $\dot{\beta}_{i,l,m} \in \mathbb{R}$ is the radar cross-section (RCS) distributed as a Chi-squared random variable with four degrees of freedom [10], $\mathbf{h}_{i,l,m,\mathrm{Rx}}$ and $\mathbf{h}_{i,l,m,\mathrm{Tx}}$ denote the channel from Tx/Rx to UE, respectively. Considering non-uniform spherical wave model [11], the element of the channel vectors $h_{i,l,m,n,\mathrm{Tx}}$ and $h_{i,l,m,n,\mathrm{Rx}}$ are expressed as

$$h_{i,l,m,n,\mathrm{Tx}} = \frac{1}{\sqrt{\alpha_{i,l,m,n,\mathrm{Tx}}}} \exp\!\Big(-\imath\frac{2\pi}{\lambda_m}\big\|\mathbf{p}'_{n,\mathrm{Tx}} - \mathbf{p}_{i,l}\big\|\Big) \tag{4}$$

$$h_{i,l,m,n,\mathrm{Rx}} = \frac{1}{\sqrt{\alpha_{i,l,m,n,\mathrm{Rx}}}} \exp\!\Big(-\imath\frac{2\pi}{\lambda_m}\big\|\mathbf{p}'_{n,\mathrm{Rx}} - \mathbf{p}_{i,l}\big\|\Big) \tag{5}$$

where $\mathbf{p}'_{n,\mathrm{Tx}}$ and $\mathbf{p}'_{n,\mathrm{Rx}}$ are the n-th antenna position of Tx and Rx for $n \in \{1, 2, \ldots, N\}$ respectively, $\alpha_{i,l,m,n,\mathrm{Tx}}$ and $\alpha_{i,l,m,n,\mathrm{Rx}}$ are the path loss, and λ_m is the wavelength of the m-th subcarrier. The path loss $\alpha_{i,l,m,n,\mathrm{Tx}}$ and $\alpha_{i,l,m,n,\mathrm{Rx}}$ follows [12]:

$$\alpha_{i,l,m,n,\mathrm{Tx}} = \Big(\frac{4\pi}{\lambda_m}\big\|\mathbf{p}'_{n,\mathrm{Tx}} - \mathbf{p}_{i,l}\big\|\Big)^2 \tag{6}$$

$$\alpha_{i,l,m,n,\mathrm{Rx}} = \Big(\frac{4\pi}{\lambda_m}\big\|\mathbf{p}'_{n,\mathrm{Rx}} - \mathbf{p}_{i,l}\big\|\Big)^2 . \tag{7}$$

According to (6) and (7), signal paths characterized by more than one bounce are neglected due to severe path loss.

For the noise $\boldsymbol{\eta}_{k,m} \sim \mathcal{CN}\left(\mathbf{0}_{N\times 1}, \sigma_\eta^2 \mathbf{I}_{N\times N}\right)$, its variance for each subcarrier is $\sigma_\eta^2 = k_\mathrm{B} T \Delta_\mathrm{f} F$, where $k_\mathrm{B} = 1.38 \times 10^{-23}\,(\mathrm{J/K})$ is the Boltzmann constant, T is the Kelvin temperature, Δ_f is the subcarrier spacing, and F is the noise figure of the BS [13].

III. Semantic UE Localization

The proposed semantic UE localization framework consists of two stages: position estimation through beam sweeping analysis and UE type classification via neural network inference. Position estimation extracts spatial parameters including AOD, AOA, and bi-static range from the beam-swept received signals. The classification stage then exploits aperture-dependent scattering characteristics manifested in these signals to distinguish UE types. This section details both stages.

A. UE Localization

The beam sweeping result $\mathbf{Z}_m \in \mathbb{C}^{N_\mathrm{B}\times N_\mathrm{B}}$ for the m-th subcarrier represents received power across all Tx-Rx beam pair combinations, where the first dimension corresponds to the Tx beam index and the second to the Rx beam index. By stacking $\mathbf{Z}_m$ across all M subcarriers, a three-dimensional array $\mathbf{Z} \in \mathbb{C}^{N_\mathrm{B}\times N_\mathrm{B}\times M}$ is constructed. Applying the inverse fast Fourier transform (IFFT) along the subcarrier dimension transforms the frequency-domain information into the bi-static range domain as

$$\tilde{\mathbf{Z}} = \mathrm{IFFT}_{\mathrm{subcarrier}}(\mathbf{Z}) \in \mathbb{C}^{N_\mathrm{B}\times N_\mathrm{B}\times M} \tag{8}$$

where the third dimension now represents bi-static range bins.

To estimate the AOD from the transmitter, the received power is averaged over all Rx beam indices, yielding a matrix $\mathbf{P}_\mathrm{Tx} \in \mathbb{R}^{N_\mathrm{Tx}\times M}$

$$\mathbf{P}_\mathrm{Tx}(b_\mathrm{Tx}, k) = \frac{1}{N_\mathrm{B}} \sum_{b_\mathrm{Rx}=1}^{N_\mathrm{B}} |\tilde{\mathbf{Z}}(b_\mathrm{Tx}, b_\mathrm{Rx}, k)|^2 \tag{9}$$

where b_Tx denotes the Tx beam index and k denotes the range bin index. Fig. 2(a) illustrates the structure of $\mathbf{P}_\mathrm{Tx}$, which represents the average power for each Tx beam across range bins. The estimated AOD $\hat{\varphi}$ and bi-static range $\hat{r}$ are obtained by identifying the peak location as

$$(\hat{b}_\mathrm{Tx}, \hat{k}) = \underset{b_\mathrm{Tx}, k}{\mathrm{argmax}}\, \mathbf{P}_\mathrm{Tx}(b_\mathrm{Tx}, k) \tag{10}$$

$$\hat{\varphi} = \phi_{\hat{b}_\mathrm{Tx}}, \quad \hat{r} = r_{\hat{k}} \tag{11}$$

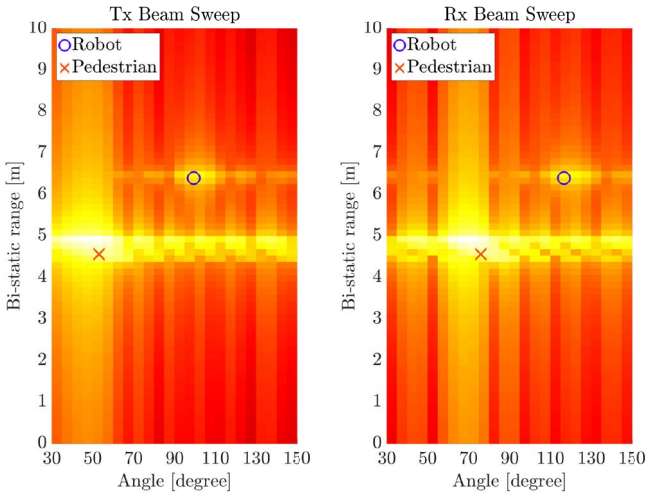

(a) Average power for Tx beam sweeping.

(b) Average power for Rx beam sweeping.

Fig. 2. Cosine similarity heatmaps for two types of extended target users.

where $\phi_{\hat{b}_{\text{Tx}}}$ is the steering angle corresponding to the $\hat{b}_{\text{Tx}}$-th Tx beam and $r_{\hat{k}}$ is the range corresponding to the $\hat{k}$-th range bin.

Similarly, averaging over Tx beam indices yields $\mathbf{P}_{\text{Rx}} \in \mathbb{R}^{N_{\text{B}} \times M}$ for AOA estimation:

$$\mathbf{P}_{\text{Rx}}(b_{\text{Rx}}, k) = \frac{1}{N_{\text{B}}} \sum_{b_{\text{Tx}}=1}^{N_{\text{B}}} |\tilde{\mathbf{Z}}(b_{\text{Tx}}, b_{\text{Rx}}, k)|^2. \tag{12}$$

The estimated AOA $\hat{\theta}$ is determined by:

$$\hat{b}_{\text{Rx}} = \underset{b_{\text{Rx}}}{\operatorname{argmax}} \mathbf{P}_{\text{Rx}}(b_{\text{Rx}}, k), \quad \hat{\varphi} = \phi_{\hat{b}_{\text{Rx}}}. \tag{13}$$

These estimated parameters $(\hat{\varphi}, \hat{\theta}, \hat{r})$ characterize the UE position relative to the transceiver system.

B. UE Classification

Different UE types exhibit distinct scattering characteristics due to their varying physical dimensions. As illustrated in Fig. 2, the power spectrum for a robot with 0.1 m aperture width shows sharper and more localized features, while a pedestrian with 0.6 m aperture width produces broader spectral spreading in both Tx and Rx beam sweeping results. This difference in spectral spreading arises from the aperture-dependent scattering properties, where larger physical dimensions result in more distributed angular reflections.

To exploit these distinguishable features for classification, the proposed method constructs an input feature vector by concatenating the Tx and Rx beam sweeping power profiles. Specifically, the power matrices $\mathbf{P}_{\text{Tx}} \in \mathbb{R}^{N_{\text{B}} \times M}$ and $\mathbf{P}_{\text{B}} \in \mathbb{R}^{N_{\text{Rx}} \times M}$ obtained from (9) and (12) are flattened and concatenated to form the input feature vector $\mathbf{x} \in \mathbb{R}^{2N_{\text{B}} \times M}$. This vector encodes the spatial-spectral characteristics across both transmit and receive angular domains.

Algorithm 1: Semantic UE localization

Input : Beam sweeping result
Output: Estimated AOD, estimated AOA, estimated TOA, and classification result

1 Beam sweeping;
2 Measure beam sweeping results as (1);
3 Perform IFFT as (8);
4 Compute power matrices as (9) and (12);
5 Estimate $(\hat{\varphi}, \hat{\theta}, \hat{r})$ following (11) and (13);
6 Classify UE type as (14);

A neural network classifier $f_\omega(\cdot)$ with learnable parameters ω maps the input features to UE type probabilities:

$$\hat{\mathbf{y}} = f_\omega(\mathbf{x}) \tag{14}$$

where $\hat{\mathbf{y}} \in [0,1]^C$ represents the predicted probability distribution over C UE classes (human and robot in this work). The network is trained using the cross-entropy loss function

$$\mathcal{L}(\omega) = -\frac{1}{D} \sum_{d=1}^{D} \sum_{c=1}^{C} y_d^{(c)} \log(\hat{y}_d^{(c)}) \tag{15}$$

where D is the number of training samples, $y_d^{(c)}$ is the ground truth label, and $\hat{y}_d^{(c)}$ is the predicted probability for class c of the n-th sample. The predicted UE type is determined by $\hat{c} = \operatorname{argmax}_c \hat{y}^{(c)}$. By training on diverse scenarios with varying UE positions and types, the classifier learns to distinguish aperture-dependent scattering signatures, enabling semantic localization that jointly provides position estimates and UE type classification. Algorithm 1 summarizes the overall procedure for semantic UE localization.

IV. Case Studies

This section validates the proposed semantic UE localization method through comprehensive simulations configured with a practical mmWave transceiver system specification. Table I summarizes the key simulation parameters and the classification network architecture.

A. Localization Performance

Fig. 3 illustrates the angle estimation root-mean-square error (RMSE) as a function of beam spacing angle for both robot and pedestrian UE types. Since AOA and AOD estimation exhibit similar RMSE values, their average is presented for clarity. The results demonstrate that narrower beam spacing yields significantly improved angle estimation accuracy, as finer angular resolution enables more precise identification of peak locations in the beam sweeping power matrix. Notably, pedestrians with 0.6 m aperture width consistently exhibit higher RMSE compared to robots with 0.1 m aperture width. This performance degradation stems from the broader spectral spreading caused by larger physical dimensions, which reduces the sharpness of the spatial power profile and consequently diminishes localization precision.

TABLE I
SIMULATION PARAMETERS

Parameter	Description	Value
N	Number of antenna	8
-	Carrier frequency	28 GHz
M	Number of subcarriers	800, 1600, …, 4000
P_{T}	Transmit power	23 dBm
L	Number of users	2
T	Kelvin temperature	290
Δ_{f}	Subcarrier spacing	480 kHz
F	Noise figure	7 dBm
D	Number of training samples	2000
-	Learning rate	0.001
-	Training epoch	100
Layer	**Parameters**	**Activation**
Input	Shape: $(2N_{\mathrm{B}}, M, 1)$	–
Flatten	–	–
Dense	Units: 1000	ReLU
Dense	Units: 1000	ReLU
Dense	Units: 2	Softmax

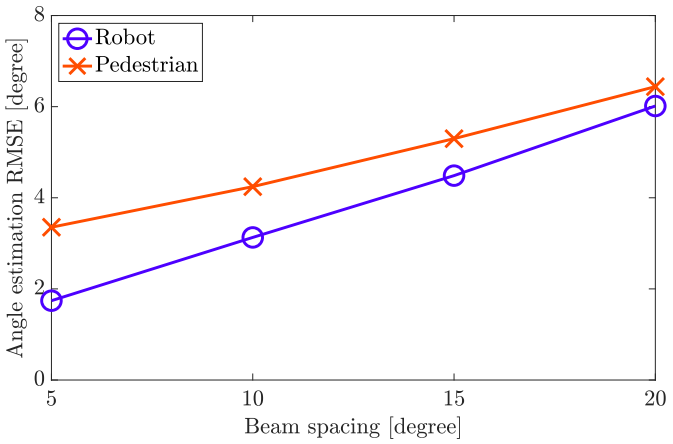

Fig. 3. AOA, AOD estimation RMSE over beam spacing.

Fig. 4 presents the bi-static range estimation RMSE versus bandwidth, with the beam spacing angle held constant. The number of subcarriers varies from 800 to 4000, corresponding to proportionally increasing total bandwidth. As expected, wider bandwidth provides enhanced range resolution through finer delay discrimination capability in the IFFT-transformed range domain. Similar to angle estimation, pedestrians demonstrate higher range estimation RMSE than robots across all bandwidth configurations, reinforcing the observation that larger aperture dimensions degrade localization accuracy for both angular and range parameters.

B. Classification Performance

Fig. 5 depicts the UE type classification accuracy as a function of training epochs. The classifier converges to approximately 80 % accuracy for both pedestrian and robot types, demonstrating effective discrimination of aperture-dependent

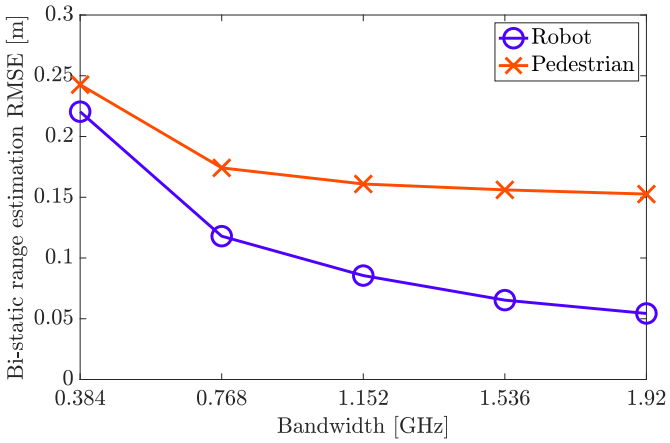

Fig. 4. Bi-static range estimation RMSE over bandwidth.

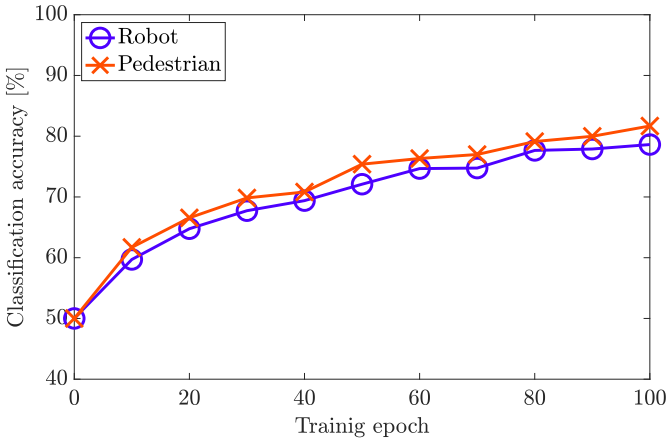

Fig. 5. Classification accuracy for extended target users.

scattering characteristics from single-snapshot beam sweeping measurements. While 80 % accuracy represents promising performance given the challenging single-observation scenario, the result reveals substantial potential for improvement through temporal fusion of multiple snapshots. Aggregating observations across multiple time instances would enable more robust feature extraction and statistical averaging, likely driving classification accuracy toward higher levels.

The combined results validate that the proposed method effectively performs joint localization and classification across different UE types. The framework successfully extracts position-related parameters (AOD, AOA, bi-static range) while simultaneously distinguishing UE types through learned scattering signatures, demonstrating feasibility for radio-based semantic environmental awareness.

V. Conclusion

This paper proposed a semantic UE localization framework for OFDM transceiver systems with analog beamforming that simultaneously estimates position and classifies UE type by exploiting aperture-dependent scattering characteristics. The

method employs beam sweeping at the transmitter and receiver to extract AOD, AOA, and bi-static range information, with a neural network classifier distinguishing UE types based on their distinct scattering patterns. Simulations configured with practical mmWave transceiver system specifications validated the framework, demonstrating that narrower beam spacing and wider bandwidth improve localization accuracy, while larger physical apertures produce broader spectral spreading that degrades localization precision but enables effective classification at approximately 80 % accuracy from single-snapshot measurements. This performance reveals substantial potential for improvement through temporal fusion of multiple observations, enabling radio-based semantic environmental awareness essential for location-based services and digital twin construction in next-generation wireless networks.

REFERENCES

[1] Y. Xiao, Y. Liao, Y. Li, G. Shi, H. V. Poor, W. Saad, M. Debbah, and M. Bennis, "Reasoning over the air: A reasoning- based implicit semantic-aware communication framework," *IEEE Trans. Wireless Commun.*, vol. 23, no. 4, pp. 3839–3855, Apr. 2024.

[2] S. K. Jagatheesaperumal, Z. Yang, Q. Yang, C. Huang, W. Xu, M. Shikh-Bahaei, and Z. Zhang, "Semantic-aware digital twin for metaverse: A comprehensive review," *IEEE Wireless Commun.*, vol. 30, no. 4, pp. 38–46, Aug. 2023.

[3] S. K. Dehkordi, L. Pucci, P. Jung, A. Giorgetti, E. Paolini, and G. Caire, "Multistatic parameter estimation in the near/far field for integrated sensing and communication," *IEEE Trans. Wireless Commun.*, vol. 23, no. 12, pp. 17 929–17 944, Dec. 2024.

[4] Y. Lin, S. Jin, M. Matthaiou, and X. You, "Channel estimation and user localization for irs-assisted mimo-ofdm systems," *IEEE Trans. Wireless Commun.*, vol. 21, no. 4, pp. 2320–2335, Apr. 2022.

[5] H. Park, J. Kang, S. Lee, J. W. Choi, and S. Kim, "Deep Q-network based beam tracking for mobile millimeter-wave communications," *IEEE Trans. Wireless Commun.*, vol. 22, no. 2, pp. 961–971, Feb. 2023.

[6] J. Chen, K. Yao, and R. Hudson, "Source localization and beamforming," *IEEE Signal Process. Mag.*, vol. 19, no. 2, pp. 30–39, Mar. 2002.

[7] H. Park, H. Chung, A. Conti, M. Z. Win, and S. Kim, "Robust near-field beam tracking via deep Q-network for THz communications," in *Proc. IEEE 27th Int. Conf. Inf. Fusion*, Jul. 2024, pp. 1–5.

[8] Z. Du, F. Liu, and Z. Zhang, "Sensing-assisted beam tracking in V2I networks: Extended target case," in *Proc. IEEE Int. Conf. Acoust., Speech, Signal Process. (ICASSP)*, 2022, pp. 8727–8731.

[9] A. Vaccari, M. Z. Win, and A. Conti, "Tracking and identification of targets via mmWave MIMO radar," in *Proc. IEEE Mil. Commun. Conf. (MILCOM)*, Oct. 2024, pp. 336–341.

[10] M. I. Skolnik *et al.*, *Introduction to radar systems*. McGraw-hill New York, 1980, vol. 3.

[11] Y. Liu, Z. Wang, J. Xu, C. Ouyang, X. Mu, and R. Schober, "Near-field communications: A tutorial review," *IEEE Open J. Commun. Society*, vol. 4, pp. 1999–2049, Aug. 2023.

[12] *Technical Specification Group Radio Access Network; Study on Channel Model for Frequencies From 0.5 to 100 GHz*. document TR 38.901 V18.0.0, Release 18, Mar. 2024.

[13] H. Nyquist, "Thermal agitation of electric charge in conductors," *Phys. Rev.*, vol. 32, pp. 110–113, Jul. 1928.